

ELROND: Exploring and decomposing intrinsic capabilities of diffusion models

Paweł Skierski^{1,2} Tomasz Trzcinski^{1,2} Kamil Deja^{1,2}

Abstract

A single text prompt passed to a diffusion model often yields a wide range of visual outputs determined solely by stochastic process, leaving users with no direct control over which specific semantic variations appear in the image. While existing unsupervised methods attempt to analyze these variations via output features, they omit the underlying generative process. In this work, we propose a framework to disentangle these semantic directions directly within the input embedding space. To that end, we collect a set of gradients obtained by backpropagating the differences between stochastic realizations of a fixed prompt that we later decompose into meaningful steering directions with either Principal Components Analysis or Sparse Autoencoder. Our approach yields three key contributions: (1) it isolates interpretable, steerable directions for precise, fine-grained control over a single concept; (2) it effectively mitigates mode collapse in distilled models by reintroducing lost diversity; and (3) it establishes a novel estimator for concept complexity under a specific model, based on the dimensionality of the discovered subspace.

1. Introduction

Text-to-image diffusion models (Rombach et al., 2022) are capable of generating remarkable visual variations from a single prompt, yet the fundamental limitation is that when interacting with those models, their capabilities are only observable through the trial-and-error approach with multiple generations from random seeds and altered prompts. This opacity stems from the fact that textual prompts are inherently under-determined. A single prompt such as "An image of a monster" often corresponds to a vast manifold of potential outputs, selected into particular instantiation on the basis of stochastic initialization. Consequently, what

¹Warsaw University of Technology Research Institute. Correspondence to: Paweł Skierski <pawel.skiers.dokt@pw.edu.pl>.

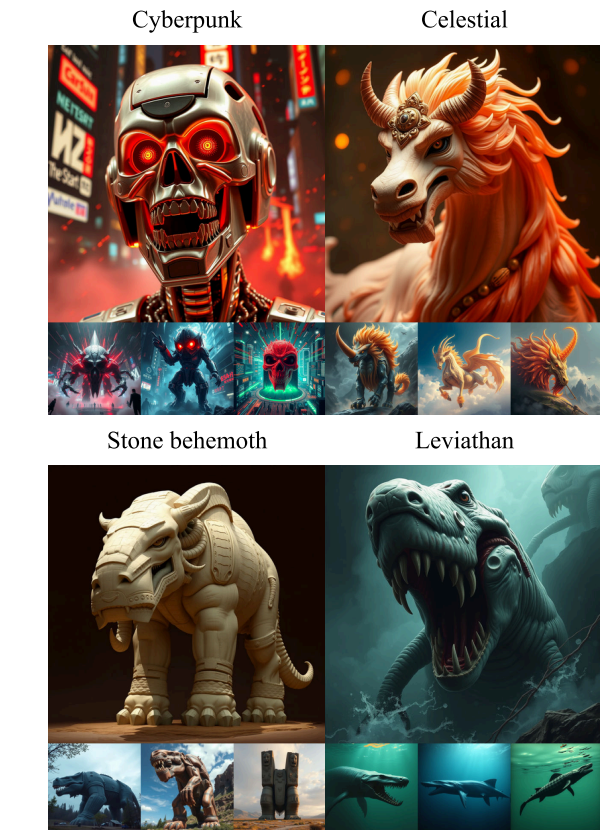


Figure 1. Unsupervised Discovery of Latent Directions. ELROND is able to extract, in an unsupervised way, latent directions that allow for exploration of the visual capabilities of the diffusion model. We visualize four directions extracted for a concept *monster* from Flux Schnell (BlackForestLabs, 2024).

appears to the user as random noise, turns into a selection mechanism for a specific, yet unlabeled semantic attributes.

Existing unsupervised methods (Gandikota et al., 2025) automatically decompose those capabilities by analyzing the visual features of generated samples. These methods typically employ techniques like PCA on visual embeddings (e.g., CLIP (Radford et al., 2021)) to identify the axes of image variations. In this work, we argue for a more direct approach. Instead of categorizing the possible options given a set of generated outputs, we propose to decompose possible directions truly reachable by the diffusion model in the text embedding space itself.

Implementing this direct approach, however, reveals a fundamental limitation of currently used mechanistic interpretability tools like linear probings or sparse autoencoders which operate on intermediate activations to find semantic features. While doing so, they typically rely on diverse prompts to generate the necessary variance. However, when exploring the intrinsic capabilities of a single concept, the text conditioning has to remain static across generations. Consequently, the standard forward-pass activations exhibit no variance, rendering traditional decomposition methods ineffective for isolating the semantic directions within the text embedding space.

In this work, we propose to bridge this gap and analyze the local geometry of the embedding space by isolating the signals required to transition between distinct stochastic realizations of the same prompt. In order to do so, we propose to backpropagate the difference between these realizations to the specific concept token in the text embedding space. This process captures the gradient vectors that map the trajectories between random seeds, effectively recovering the tangent space of the concept manifold. For instance, given the prompt "An image of a monster", we identify a gradient direction in the embedding space that steers the generation from a randomly generated "*water leviathan*" into another random generation resulting in "*stone behemoth*".

To structure these signals, we aggregate a collection of such gradient vectors and decompose them into meaningful directions. We evaluate two distinct decomposition strategies: Principal Component Analysis (PCA), which identifies a set of orthogonal axes encoding the most significant variations in the concept, and Sparse Autoencoders (SAE) (Olshausen & Field, 1997), which disentangle the gradients into sparse, monosemantic features representing specific attributes.

We validate our framework through three primary applications. First, we demonstrate precise semantic steering: by adding the discovered directions to the embeddings during sampling, we can deterministically guide the generation toward desired characteristics as presented in Figure 1. Crucially, unlike existing methods, our approach facilitates precise token-level composability, enabling the independent steering of distinct concepts within a complex scene. Secondly, by applying our method to distilled versions of the model, we are able to successfully mitigate mode collapse by reintroducing the lost diversity to the model. We demonstrate effective mitigation using steering directions calculated from either the original teacher model or directly from the distilled model itself. Finally, we introduce a novel estimator for concept complexity, defined as the Local Intrinsic Dimensionality (LID) of the discovered semantic subspace, which enables us to compare the relative complexity of different concepts within a diffusion model.

Our contribution can be summarized as follows:

- We introduce a new method for unsupervised decomposition of concepts learned by diffusion models
- We validate our approach, showing that it can be used for precise steering of the generative process, facilitating effective composition and improving the diversity
- On the basis of the discovered semantic subspace, we define a new metric of the concept complexity

2. Related Work

Precise generation in text-to-image diffusion models

Achieving desired control over generated images necessitates mechanisms that go beyond text prompting. Standard approaches typically introduce additional conditioning by extending the model through adapters (ControlNet (Zhang et al., 2023), T2I-Adapter (Mou et al., 2024)). Without affecting the structure of the model architecture, Rodriguez et al. (2024; 2025) have introduced a framework enabling fine-grained control by transporting the activations during inference. Alternatively, attention-based methods like Prompt-to-prompt (Hertz et al., 2022) or Ledit++ (Brack et al., 2023) leverage cross-attention maps of a reference generation to localize changes, while Mokady et al. (2022) optimizes a text-conditioning space. Most relevant to our proposed methodology, Baumann et al. (2025) identifies semantic directions within the CLIP text embeddings by backpropagating the difference in noise predictions between contrastive prompts (e.g., *young person* vs. *old person*). However, this reliance on manually constructing contrastive pairs necessitates *a priori* knowledge of the target attributes, rendering it infeasible for the unsupervised discovery of unknown semantic variations.

Unsupervised concepts discovery Without supervision, Kwon et al. (2022) identify that U-net's bottleneck features possess a semantic structure, while Dalva & Yanardag (2024) employs contrastive learning on the directions added to the intermediate diffusion steps, to identify steerable directions. Similarly, Liu et al. (2023) decompose image into a set of randomly initialized concepts that can sum up into the observed composition by the summation of individual score functions. On the other hand, building on the model adaptation techniques, Gandikota et al. (2024; 2025) automated the discovery process by applying PCA to the semantic embedding space of generated images, discovering orthogonal and controllable basis vectors for a given concept without manual attribute specification. From a conceptually different direction, Dravid et al. (2024) interpreted the semantically meaningful direction in the model's weight space.

Sparse Autoencoders in Diffusion Models Recent research has successfully adapted Sparse Autoencoders (SAE) to interpret text-to-image diffusion models. Works

by Cywiński & Deja (2025); Surkov et al. (2024); Huang et al. (2025) demonstrate that SAEs can decompose activations of diffusion models into interpretable features, allowing for precise steering of the generative process. In parallel, some works apply SAEs to interpret CLIP embeddings (Pach et al., 2025; Dreyer et al., 2025) with additional applications when this model is used as conditioning for diffusion models (Kim et al., 2024; Ye et al., 2025), including precise edition as shown by Kamenetsky et al. (2025). In this work, we apply SAE to the gradients of the text embeddings to capture the variance between stochastic realizations of the single concept defined by one prompt.

Measuring the complexity of generations Local Intrinsic Dimension (LID) quantifies the geometric complexity of a data representation. Formally, assuming the data resides on a manifold \mathcal{M} embedded in a high-dimensional space, the LID at a point x corresponds to the dimension of the tangent space $T_x\mathcal{M}$. Tempczyk et al. (2022) introduced LIDL, a method for estimating LID by leveraging the rate of change of likelihood estimates from parametric density estimators under varying noise levels. Building on this, Kamkari et al. (2024) proposed FLIPD, which utilizes the Fokker-Planck equation to provide a more efficient and accurate LID estimator. Similarly, Stanczuk et al. (2022) demonstrate that diffusion models implicitly encode the data manifold’s dimension. In a parallel line of work, Lu et al. (2025) explore Variational Sparse Autoencoders (vSAE) to model low-dimensional latent structures. In contrast to methods analyzing the data manifold, we estimate the dimensionality of the concept manifold within the text embeddings to quantify complexity of the concept’s representation as learned by the diffusion model.

3. Motivation: Linearity in Semantic Latent Spaces

To ground our methodological approach, we first investigate the geometric structure of the semantic transformations within the diffusion model’s embedding space. Recent unsupervised methods have successfully demonstrated that analyzing the variance of visual embeddings (e.g., CLIP) from generated images can recover meaningful control directions. These approaches implicitly rely on the assumption that semantic variations can be approximated as linear directions within the output embedding space. To explore the limits of this approximation, we analyze the geometry of a known, continuous semantic transition.

First, we simulate a “ground truth” semantic direction by linearly interpolating between the text embeddings of two concepts, $c_{start} = \text{“Person”}$ and $c_{end} = \text{“Old person”}$. We then generate sequences of images $\{x_t\}$ by conditioning the diffusion model on $c_t = (1-t)c_{start} + tc_{end}$ for $t \in [0, 1]$,

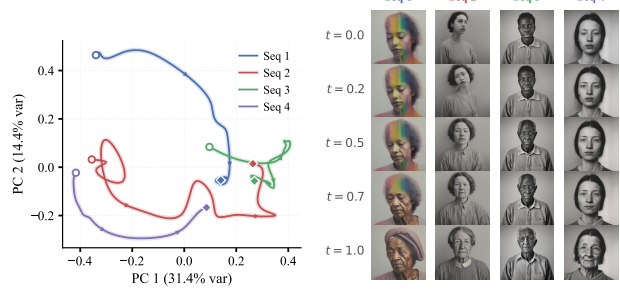


Figure 2. Semantic trajectories within DM conditioning space. Semantics transitions in the diffusion model outputs resulting from linear interpolation (right) do not correspond to a linear direction within CLIP embedding space (left) (first 2 PCA dimensions). (Solid markers denote the final state ($t = 1.0$), hollow circles indicate the initialization ($t = 0$), curves are smoothed using cubic spline interpolation).

while keeping the added noises fixed. Finally, we project the resulting image sequences into the CLIP visual embedding space. As shown in Figure 2 (left), the trajectories do not follow a linear path between the start and end states, but instead exhibit significant curvature. We quantify this by measuring the Straightness Index of the trajectory, which yields a low value of 0.17 (far below the ideal linear value of 1.0) and an Average Cosine Similarity of -0.47 between consecutive step vectors. This indicates that a linear interpolation in the text conditioning space maps to a highly complex, non-linear trajectory in the visual embedding space (see Appendix A for full metrics).

Despite this geometric complexity, Figure 2 (right) confirms that visual progression remains perceptually smooth and coherent. These findings reveal that the diffusion model performs a highly non-linear projection from the learned semantic manifold to the external visual embedding space. This motivates our proposed method: by shifting our analysis from the output analyses to the gradients within the conditioning space, we aim to recover the local, disentangled signals that drive these transformations directly within the manifold of the usable text-embeddings.

4. Method

In this section, we describe our method for the decomposition of semantic directions in text-to-image diffusion models as outlined in Figure 3. First, we collect a set of gradients located in the textual embedding space, which we then decompose into individual vectors. Finally, we use the primitive directions for precise steering, and the dimensionality of the decomposed space as the concept complexity estimator.

4.1. Collecting Semantic Gradients

To decompose the intrinsic capabilities of a diffusion model, we propose to first identify the subspace of the embedding space that governs the variations of a specific concept. We

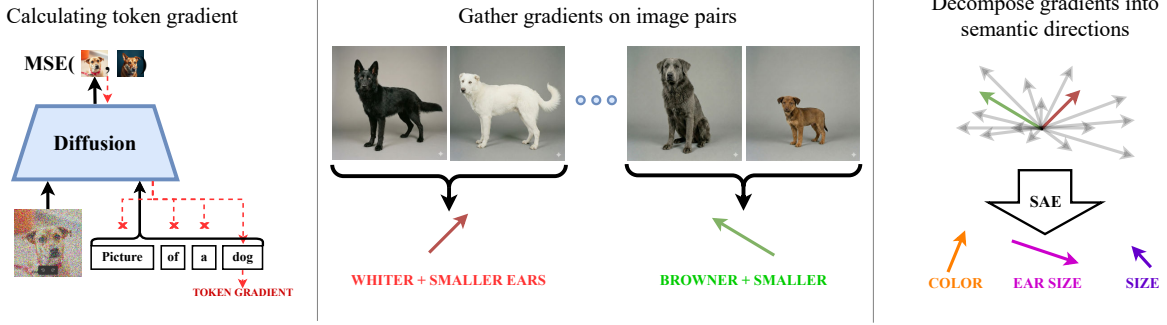


Figure 3. To extract the latent directions for a given concept, we backpropagate the differences between image instances generated from the same prompt to the given token. We then disentangle the latent directions by training SAE / computing PCA on the gradients.

posit that a concept c resides on a learned low-dimensional manifold \mathcal{M} within the high-dimensional text embedding space. Our objective is to empirically approximate the tangent space $T_{e_{tok}}\mathcal{M}$ at the concept’s embedding – effectively spanning the directions of valid semantic variation available to the model. We achieve this by collecting gradients that map the trajectories between different stochastic realizations of the concept. Let P be a concept prompt (e.g., “A picture of a *monster*”) containing a token of interest tok and embeddings $e_{tok} \in \mathbb{R}^d$. We first sample a dataset of N images, $\mathcal{X} = \{x^{(1)}, \dots, x^{(N)}\}$, representing this concept.

To extract a single gradient, we sample a pair of distinct images $(x^{(i)}, x^{(j)})$ from \mathcal{X} . We encode $x^{(i)}$ into latent space to obtain $z_0^{(i)}$ and apply forward diffusion to a noise level t :

$$z_t^{(i)} = \alpha_t z_0^{(i)} + \sigma_t \epsilon, \quad \epsilon \sim \mathcal{N}(0, I). \quad (1)$$

Crucially, at any timestep t , an estimate of the clean latent \hat{z}_0 can be predicted from the current noisy state z_t and the model prediction:

$$\hat{z}_0(z_t, t, c) = \frac{z_t - \sigma_t \epsilon_\theta(z_t, t, c)}{\alpha_t}. \quad (2)$$

Therefore, we predict the clean latent \hat{z}_0 from $z_t^{(i)}$ and compute the standard diffusion reconstruction loss (MSE) between this prediction and the *second* image $x^{(j)}$:

$$\mathcal{L}_{sem} = \|\hat{z}_0(z_t^{(i)}, t, c) - z_0^{(j)}\|_2^2. \quad (3)$$

(see Appendix G for alternative formulations with other loss functions) We backpropagate this loss to the text embedding space and extract the gradient with respect to the embedding of the token of interest, e_{tok} :

$$g_{i,j} = \nabla_{e_{tok}} \mathcal{L}_{sem}. \quad (4)$$

Intuitively, minimizing this loss forces the model to alter its conditioning c such that the output shifts from the characteristics of $x^{(i)}$ toward $x^{(j)}$. By repeating this process for many pairs, we collect a dataset of gradients $\mathcal{G} = \{g_1, \dots, g_M\}$, representing the semantic directions that span the manifold of the concept in the embedding space.

4.2. Discovering Latent Directions

The raw gradients in \mathcal{G} often contain entangled information about several semantic changes together with unimportant noise. To extract disentangled, semantic directions, we decompose the distribution of gradients with two approaches:

Principal Component Analysis (PCA). We perform PCA on \mathcal{G} . The resulting latent directions are defined as the principal components (eigenvectors) v_k . To filter out noise, we retain only components with explained variance above a threshold τ .

Sparse Autoencoder Decomposition. For more interpretable directions, we train a Top-k Sparse Autoencoder (SAE) (Bussmann et al., 2024) on the set of gradients \mathcal{G} . To that end, we use a model composed of two neural networks: an encoder and a decoder trained using a reconstruction loss with sparsity constraints. Given an input vector $v \in \mathbb{R}^d$, the encoder projects it to a higher-dimensional latent space $h \in \mathbb{R}^n$ using a linear transformation followed by a TopK activation function:

$$h = \text{TopK}(W_{enc}(v - b_{pre})), \quad (5)$$

where $W_{enc} \in \mathbb{R}^{n \times d}$ is the encoder weight matrix, $b_{pre} \in \mathbb{R}^d$ is a pre-encoder bias, and $\text{TopK}(\cdot)$ is a non-linearity that retains only the k largest activation values, setting the rest to zero. This architectural constraint enforces a strict sparsity level of k active features per input.

The decoder then reconstructs the input from the sparse latent code h , and minimize the reconstruction error:

$$\mathcal{L}_{SAE} = \|v - W_{dec}h + b_{pre}\|_2^2. \quad (6)$$

where $W_{dec} \in \mathbb{R}^{d \times n}$ is the decoder weight matrix. The model is trained to minimize the reconstruction error:

Post-training, we identify the set of „alive” latent features (with non-zero activation density). The decoder weights corresponding to these features, $d_k = (W_{dec})_{:,k}$, represent the disentangled semantic directions. The sparsity constraint ensures that these directions represent fundamental, primitive attributes of the concept.

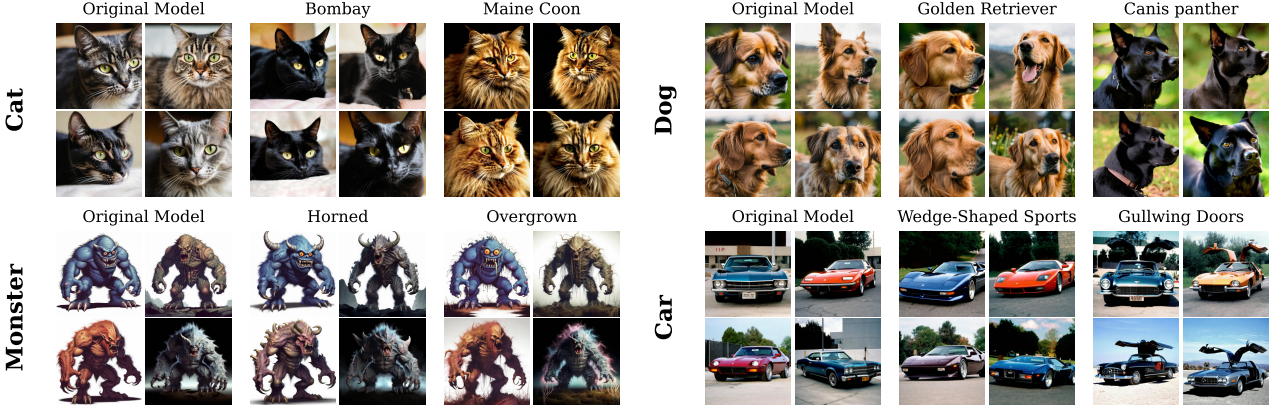


Figure 4. ELROND decomposes the visual capabilities of the diffusion model. We show latent directions discovered in SDXL-DMD.

4.3. Semantic Steering

Given a discovered latent direction d (derived either from PCA or SAE), we can precisely steer the generation process to obtain a final generation with a characteristic defined by a given direction. For a given prompt, let e_{tok} be the original embedding of the concept token. We modulate the embedding by injecting the latent direction:

$$e'_{tok} = e_{tok} + \lambda \cdot d, \quad (7)$$

where $\lambda \in \mathbb{R}$ is a strength parameter. The modified embedding is then passed to the diffusion model. This method scales naturally to complex prompts with multiple subjects, as directions are derived relative to specific tokens. Consequently, we can apply distinct directions to different subjects simultaneously with limited cross-concept interference.

4.4. Concept Complexity Estimation

As detailed in Section 4.1, the collected gradients \mathcal{G} approximate the tangent space $T_{e_{tok}}\mathcal{M}$ of the learned concept manifold, effectively spanning the directions of valid semantic variation recognized by the model.

Consequently, we propose to estimate the local intrinsic dimension (LID) of the concept manifold by analyzing the dimensionality of the subspace spanned by \mathcal{G} . Using the PCA of the gradient matrix, we calculate the number of components with variance exceeding a noise floor ϵ . This value serves as a proxy for *concept complexity*, quantifying the richness and diversity of the concept as understood by the diffusion model. A higher dimensionality implies a complex concept with many degrees of freedom (e.g., "human"), while a lower dimensionality implies a constrained, simple concept (e.g., "cube").

5. Experiments

In this section, we empirically validate our method’s ability to decompose semantic concepts into steerable directions.

5.1. Experimental Setup

We conduct our main experiments using the SDXL (Podell et al., 2023) model and its distilled version SDXL-DMD (Yin et al., 2024), but we also show how ELROND generalizes to transformer-based Flux Schnell (BlackForest-Labs, 2024) in the Appendix D. In both architectures, the text conditioning acts as a concatenation of embeddings from CLIP and T5 encoders. Consequently, our method operates directly on this joint embedding space (dim=2048 for SDXL, dim=4096 for Flux). To analyze a specific concept c , we employ a generic prompt template $P = \text{"A picture of } \langle c \rangle\text{"}$. For each concept, we sample $N = 10,000$ images using the base model and collect 30,000 semantic gradients as described in Section 4. Empirically, we find that when collecting gradients, setting t to the highest noise level (i.e., $t \approx T$) yields the most semantically rich gradients, as the model relies almost entirely on the text conditioning c to restructure the image (see Appendix C for more details). For the decomposition step via Principal Component Analysis (PCA), we empirically establish a significance threshold of $\tau = 2.5/d_{embed}$, where d_{embed} is the dimensionality of the text embedding space. For SAE training, we use $k = 32$ and $d = d_{embed}$.

5.2. Concept Decomposition

First, we demonstrate that our method can serve as an unsupervised tool for decomposing high-level concepts into primitive semantic directions that align with the diffusion model’s internal representations. To that end, following (Gandikota et al., 2025), we apply our method to a set of concepts, extract the interpretable latent directions, and use them to steer the generation process. As visualized in Figure 4, the discovered directions correspond to distinct, semantically coherent attributes. For more examples and details on the discovered subspaces see Appendix F.

A robust decomposition method should not only identify attributes but also enable the exploration of the model’s full

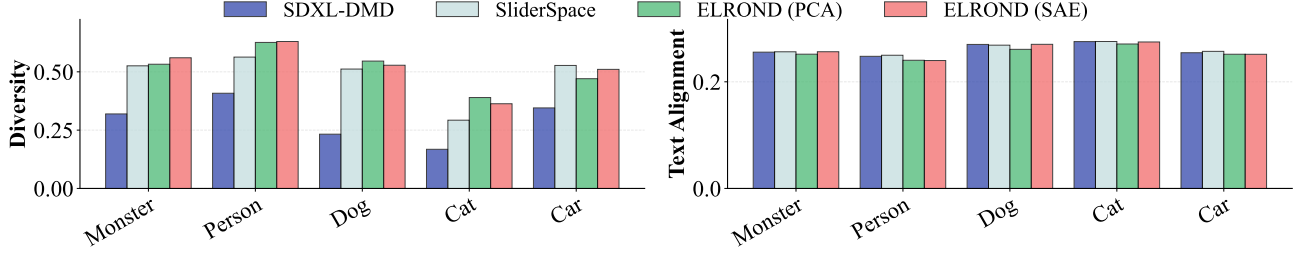


Figure 5. ELROND generates visually diverse variations of concepts (left) as measured by mean DreamSim distance (higher is better). Despite this, it maintains similar text-to-image alignment (right), as measured by CLIP Scores (lower is better).

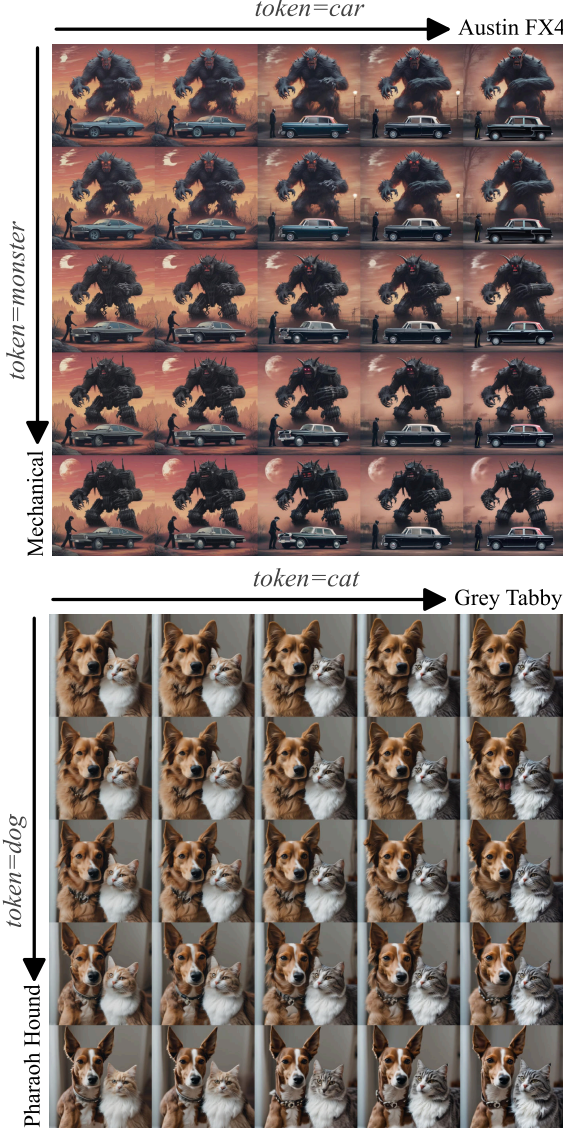


Figure 6. Applying latent directions discovered by ELROND allows for a token-level composability, enabling independent steering of distinct concepts.

potential. To quantify this, we evaluate the diversity of images generated by modulating the concept embedding with our discovered directions. For a given concept, we generate 10,000 images where, for each sample, we modify the

concept token embedding by adding a linear combination of 3 randomly selected latent directions. We measure the intra-class diversity using the DreamSim distance (Fu et al., 2023) and assess semantic consistency via CLIP Score (Hessel et al., 2021). We compare our approach against the base SDXL-DMD model and SliderSpace (Gandikota et al., 2025), a state-of-the-art method for unsupervised concept decomposition. Quantitative results of this comparison are presented in Figure 5. While all the methods maintain high semantic consistency with the original prompt (Figure 5, right), ELROND yields a significantly higher diversity score than the original SDXL-DMD model across all tested concepts (Figure 5, left) and outperforms SliderSpace.

We posit that this advantage stems from the source of the semantic signal. While SliderSpace depends on an external proxy (such as CLIP) to define semantic axes, ELROND derives directions from the diffusion model’s own backpropagated gradients. This ensures that the discovered steering vectors are natively aligned with the model’s internal representations. Consequently, our method can drive the generation toward significant semantic variations without departing from the model’s learned manifold, allowing for a more comprehensive exploration of the concept space while maintaining higher generation quality than methods guided by external embeddings.

5.3. Composability and Subject-Specific Control

A critical limitation of methods operating on all activations or the whole model, such as SliderSpace, is the difficulty in isolating interventions to specific subjects within a complex scene. Because SliderSpace learns global low-rank adapters, applying a direction often affects the entire image or all instances of a class simultaneously. In contrast, our method operates directly on the embedding of individual tokens. This granularity enables precise, token-level composability, allowing us to independently steer distinct concepts within a single generation with little cross-concept interference, similarly to what was observed by Garibi et al. (2025).

To demonstrate this capability, we utilize the semantic directions discovered for the concepts *Dog*, *Cat*, *Monster*, and *Car* in SDXL. We construct prompts containing multiple subjects, such as “A picture of a cat and a dog” and

Table 1. Comparison of FID scores calculated between samples generated by SDXL and the distilled SDXL-DMD. ELROND produces a distribution the closest to that of the undistilled model’s. Using latent directions extracted from the original model further improves the FID.

Concept	ELROND SAE (SDXL)	ELROND SAE (SDXL-DMD)	ELROND PCA (SDXL-DMD)	Slider Space	SDXL- DMD
Car	25.48	26.35	26.57	31.80	37.55
Cat	19.72	19.94	23.60	21.69	38.79
Dog	24.06	25.13	32.95	38.25	50.25
Monster	95.05	99.63	107.46	136.89	103.95
Person	33.61	38.90	47.35	41.52	86.94

“A picture of a monster and a car.” We then apply distinct semantic directions to the corresponding subject tokens simultaneously. Following (Gandikota et al., 2025), we find that the structural layout of the image is largely determined in the earliest denoising steps. Consequently, we skip the application of our steering vectors for the first 5 out of 50 timesteps of the diffusion process. The results are visualized in Figure 6. Our method successfully disentangles the control of spatially distinct subjects.

5.4. Diversity Enhancement and Mode Collapse Mitigation

Having demonstrated that ELROND can effectively span the rich semantic manifold of learned concepts, we now apply this observation in a practical problem of mode collapse in distilled diffusion models (Yin et al., 2024) that can be observed as repetitive outputs with reduced variation compared to their teachers. We explore our method’s ability to mitigate this issue by reinjecting semantic diversity into the generation process.

We discover latent directions for a set of concepts using both the teacher model (SDXL) and the distilled student (SDXL-DMD). To undo mode collapse, we sample images using SDXL-DMD while modifying the prompt embedding with a linear combination of 3 random directions. We evaluate three settings: using directions discovered within SDXL-DMD by PCA and SAE, and transferring directions discovered by SAE in the base SDXL model.

Qualitative results in Figure 7 demonstrate that our method effectively reverses the mode collapse, yielding more diverse and varied samples. We quantify this improvement in Table 1 by calculating the Fréchet Inception Distance (FID) between a reference distribution of 10,000 images sampled from the base SDXL model and the distributions generated by SDXL-DMD under various control methods.

As reported in Table 1, our method (SAE) using SDXL-DMD directions achieves a lower FID than both the base distilled model and SliderSpace, indicating a closer approximation of the teacher’s distribution. Notably, using directions discovered in the base SDXL model yields the best performance overall. This suggests that the teacher model

Table 2. Mean DreamSim distance (\uparrow) between generated images before and after embedding perturbation. Modulating embeddings with our **Discovered** directions results in significant semantic changes, whereas applying **Random** directions of the same magnitude yields negligible perceptual differences.

Direction Type	Cat	Monster	Car	Dog	Person
Random	0.068	0.095	0.085	0.073	0.091
Discovered (Ours)	0.230	0.288	0.249	0.223	0.261

retains a richer semantic manifold, and our method can effectively transfer this structural knowledge to the student, restoring lost modes of variation without retraining.

Moreover, the SAE-based variant also consistently outperforms our PCA-based baseline. We attribute this to the SAE’s ability to capture the *probability density* of the concept manifold, rather than just its geometric span. While PCA identifies a linear subspace where random sampling implies a uniform distribution over the manifold’s extent, the SAE dictionary adapts to the non-uniform density of the semantic gradients. Formally, because the SAE minimizes the expected reconstruction error $\mathcal{L} = \mathbb{E}_{g \sim p(g)} \|g - \hat{g}\|^2$ over the gradient distribution $p(g)$, it naturally allocates a higher density of feature vectors to regions of the manifold where $p(g)$ is high. Consequently, sampling random directions from the SAE dictionary effectively approximates sampling from the true underlying density $p(g)$, yielding a generated distribution that better matches the reference than the geometry-only approximation of PCA.

5.5. Concept Complexity Estimation

The previous sections demonstrate effectiveness of ELROND in precise steering and mitigating the model collapse. These applications rely on two fundamental assumptions that we empirically validate in this section: first, that the discovered semantic directions faithfully lie on the learned data manifold, and second, that the estimated dimensionality of these discovered subspaces serves as a reliable proxy for a concept’s semantic specificity.

To verify that our directions lie within the tangent space of the learned manifold, we compare the impact of modulating embeddings with our discovered directions and with random vectors of equal magnitude. We posit that because the data manifold occupies a significantly lower-dimensional subspace within the high-dimensional embedding space, random vectors will predominantly lie orthogonal to the manifold and thus remain semantically inert.

As illustrated in Figure 8, modulating the embedding with a discovered direction significantly alters the semantic content of the image. In contrast, adding a random vector results in negligible visual changes. To quantify this behavior, we sample 2,000 image pairs per concept, where for each pair, we generate a base image and an image perturbed by a di-



Figure 7. By sampling a set of latent directions discovered by ELROND (SAE) in the SDXL-DMD model, and applying them to the concept token, we can mitigate mode collapse in distilled model.

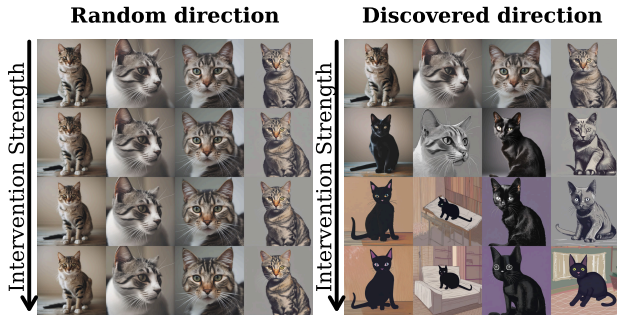


Figure 8. The diffusion model is significantly more receptive to latent embeddings found by ELROND, when compared to random directions with the same norm.

Table 3. We compare the estimated local intrinsic dimension (LID) for pairs of concepts with a clear hierarchical relationship (hyponym vs. hypernym) derived from WordNet (Miller, 1995). General concepts consistently exhibit a higher dimensionality than their specific counterparts.

Specific Concept		General Concept	
Concept	Est. LID	Concept	Est. LID
Sedan	78	Car	95
Poodle	48	Dog	65
Siamese	60	Cat	77
Woman	57	Person	68
Troll	52	Monster	74

rection. We then measure the perceptual shift using the DreamSim distance. Table 2 reports that the mean distance for images perturbed by our discovered directions is significantly higher than for those perturbed by random noise, validating our claim.

Finally, building on the geometric fidelity of ELROND’s directions, we further validate our complexity metric – the estimated Local Intrinsic Dimension (LID) – by analyzing its behavior across semantic hierarchies. Intuitively, a general concept (e.g., “Dog”) encompasses a wider range of

visual variations than a specific sub-concept (e.g., “Poodle”), and thus should correspond to a manifold of higher intrinsic dimension. To test this, we retrieve pairs of concepts with established hierarchical relationships from WordNet (Miller, 1995). We then estimate the LID for each using the numerical rank method, which calculates the number of singular values in the gradient matrix that exceed a defined noise floor as described in Section 4.4. The results in Table 3, reveal a consistent trend where the more general concept exhibits a higher LID compared to its specific counterpart, validating our metric as a proxy for semantic complexity.

6. Limitations

While ELROND effectively uncovers latent semantic directions, it is not without limitations. First, while our approach does not require model retraining, the data collection phase is computationally extensive as extracting the gradient dataset requires backpropagating through the diffusion model for thousands of image pairs. In Appendix B, we evaluate the impact of the sampled dataset on the discovered subspace. Second, as embeddings are often contextual, adding some directions to a token may influence the visual realization of another token (see Appendix E). Finally, as presented in the Appendix E, some of the directions discovered either through SAE or PCA, might not be interpretable.

7. Conclusions

We introduce ELROND, a framework for decomposing semantic concepts in diffusion models by analyzing gradients within the conditioning space. Our approach isolates steerable directions for precise control, mitigates mode collapse, and establishes a novel metric for concept complexity based on the discovered subspace. Ultimately, we provide a geometry-grounded method for interpreting and manipulating generative capabilities without supervision.

Impact Statement

This paper presents work whose goal is to advance the field of Machine Learning. There are many potential societal consequences of our work, none which we feel must be specifically highlighted here.

References

Baumann, S. A., Krause, F., Neumayr, M., Stracke, N., Sevi, M., Hu, V. T., and Ommer, B. Continuous, subject-specific attribute control in t2i models by identifying semantic directions. In *Proceedings of the Computer Vision and Pattern Recognition Conference*, pp. 13231–13241, 2025.

BlackForestLabs. Flux.1 [schnell] model card. <https://huggingface.co/black-forest-labs/FLUX.1-schnell>, 2024.

Brack, M., Friedrich, F., Kornmeier, K., Tsaban, L., Schramowski, P., Kersting, K., and Passos, A. Ledits++: Limitless image editing using text-to-image models. *arXiv preprint arXiv: 2311.16711*, 2023.

Bussmann, B., Leask, P., and Nanda, N. Batchtopk sparse autoencoders. *arXiv preprint arXiv:2412.06410*, 2024.

Cywiński, B. and Deja, K. Saeuron: Interpretable concept unlearning in diffusion models with sparse autoencoders. *arXiv preprint arXiv:2501.18052*, 2025.

Dalva, Y. and Yanardag, P. Noiseclr: A contrastive learning approach for unsupervised discovery of interpretable directions in diffusion models. In *Proceedings of the IEEE/CVF conference on computer vision and pattern recognition*, pp. 24209–24218, 2024.

Dravid, A., Gondelsman, Y., Wang, K.-C., Abdal, R., Wetzstein, G., Efros, A., and Aberman, K. Interpreting the weight space of customized diffusion models. *Advances in Neural Information Processing Systems*, 37:137334–137371, 2024.

Dreyer, M., Hufe, L., Berend, J., Wiegand, T., Lapuschkin, S., and Samek, W. From what to how: Attributing clip’s latent components reveals unexpected semantic reliance. *arXiv preprint arXiv:2505.20229*, 2025.

Fu, S., Tamir, N., Sundaram, S., Chai, L., Zhang, R., Dekel, T., and Isola, P. Dreamsim: Learning new dimensions of human visual similarity using synthetic data. *arXiv preprint arXiv:2306.09344*, 2023.

Gandikota, R., Materzyńska, J., Zhou, T., Torralba, A., and Bau, D. Concept sliders: Lora adaptors for precise control in diffusion models. In *European Conference on Computer Vision*, pp. 172–188. Springer, 2024.

Gandikota, R., Wu, Z., Zhang, R., Bau, D., Shechtman, E., and Kolkin, N. Sliderspace: Decomposing the visual capabilities of diffusion models. In *Proceedings of the IEEE/CVF International Conference on Computer Vision*, pp. 15994–16003, 2025.

Garibi, D., Yadin, S., Paiss, R., Tov, O., Zada, S., Ephrat, A., Michaeli, T., Mosseri, I., and Dekel, T. Tokenverse: Versatile multi-concept personalization in token modulation space. *ACM Transactions On Graphics (TOG)*, 44(4):1–11, 2025.

Hertz, A., Mokady, R., Tenenbaum, J., Aberman, K., Pritch, Y., and Cohen-Or, D. Prompt-to-prompt image editing with cross attention control. *arXiv preprint arXiv: 2208.01626*, 2022.

Hessel, J., Holtzman, A., Forbes, M., Le Bras, R., and Choi, Y. Clipscore: A reference-free evaluation metric for image captioning. In *Proceedings of the 2021 conference on empirical methods in natural language processing*, pp. 7514–7528, 2021.

Huang, V. S.-J., Zhuo, L., Xin, Y., Wang, Z., Wang, F.-Y., Wang, Y., Zhang, R., Gao, P., and Li, H. Tide: Temporal-aware sparse autoencoders for interpretable diffusion transformers in image generation. *arXiv preprint arXiv:2503.07050*, 2025.

Kamenetsky, R., Dorfman, S., Garibi, D., Paiss, R., Patashnik, O., and Cohen-Or, D. Saedit: Token-level control for continuous image editing via sparse autoencoder. *arXiv preprint arXiv:2510.05081*, 2025.

Kamkari, H., Ross, B. L., Hosseinzadeh, R., Cresswell, J. C., and Loaiza-Ganem, G. A geometric view of data complexity: Efficient local intrinsic dimension estimation with diffusion models. *Advances in Neural Information Processing Systems*, 37:38307–38354, 2024.

Kim, D., Thomas, X., and Ghadiyaram, D. Revelio: Interpreting and leveraging semantic information in diffusion models. *arXiv preprint arXiv:2411.16725*, 2024.

Kwon, M., Jeong, J., and Uh, Y. Diffusion models already have a semantic latent space. *arXiv preprint arXiv:2210.10960*, 2022.

Kynkänniemi, T., Karras, T., Laine, S., Lehtinen, J., and Aila, T. Improved precision and recall metric for assessing generative models. *Advances in neural information processing systems*, 32, 2019.

Liu, H., Zhang, W., Xie, J., Faccio, F., Xu, M., Xiang, T., Shou, M. Z., Perez-Rua, J.-M., and Schmidhuber, J. Faster diffusion via temporal attention decomposition. *arXiv preprint arXiv: 2404.02747*, 2024.

Liu, N., Du, Y., Li, S., Tenenbaum, J. B., and Torralba, A. Unsupervised compositional concepts discovery with text-to-image generative models. In *Proceedings of the IEEE/CVF International Conference on Computer Vision*, pp. 2085–2095, 2023.

Lu, Y., Zhu, X., He, T., and Wipf, D. Sparse autoencoders, again? *arXiv preprint arXiv:2506.04859*, 2025.

Miller, G. A. Wordnet: A lexical database for english. *Communications of the ACM*, 38(11):39–41, 1995. doi: 10.1145/219717.219748.

Mokady, R., Hertz, A., Aberman, K., Pritch, Y., and Cohen-Or, D. Null-text inversion for editing real images using guided diffusion models. *arXiv preprint arXiv:2211.09794*, 2022.

Mou, C., Wang, X., Xie, L., Wu, Y., Zhang, J., Qi, Z., and Shan, Y. T2i-adapter: Learning adapters to dig out more controllable ability for text-to-image diffusion models. In Wooldridge, M. J., Dy, J. G., and Natarajan, S. (eds.), *Thirty-Eighth AAAI Conference on Artificial Intelligence, AAAI 2024, Thirty-Sixth Conference on Innovative Applications of Artificial Intelligence, IAAI 2024, Fourteenth Symposium on Educational Advances in Artificial Intelligence, EAAI 2024, February 20-27, 2024, Vancouver, Canada*, pp. 4296–4304. AAAI Press, 2024. doi: 10.1609/AAAI.V38I5.28226. URL <https://doi.org/10.1609/aaai.v38i5.28226>.

Olshausen, B. A. and Field, D. J. Sparse coding with an over-complete basis set: A strategy employed by v1? *Vision Research*, 37:3311–3325, 1997. URL <https://api.semanticscholar.org/CorpusID:14208692>.

Pach, M., Karthik, S., Bouinot, Q., Belongie, S., and Akata, Z. Sparse autoencoders learn monosemantic features in vision-language models. *arXiv preprint arXiv:2504.02821*, 2025.

Podell, D., English, Z., Lacey, K., Blattmann, A., Dockhorn, T., Müller, J., Penna, J., and Rombach, R. Sdxl: Improving latent diffusion models for high-resolution image synthesis. *arXiv preprint arXiv:2307.01952*, 2023.

Radford, A., Kim, J. W., Hallacy, C., Ramesh, A., Goh, G., Agarwal, S., Sastry, G., Askell, A., Mishkin, P., Clark, J., Krueger, G., and Sutskever, I. Learning transferable visual models from natural language supervision. *arXiv preprint arXiv: 2103.00020*, 2021.

Rodriguez, P., Blaas, A., Klein, M., Zappella, L., Apostoloff, N., Cuturi, M., and Suau, X. Controlling language and diffusion models by transporting activations. *arXiv preprint arXiv:2410.23054*, 2024.

Rodriguez, P., Klein, M., Gualdoni, E., Maiorca, V., Blaas, A., Zappella, L., Suau, X., et al. Lineas: End-to-end learning of activation steering with a distributional loss. In *The Thirty-ninth Annual Conference on Neural Information Processing Systems*, 2025.

Rombach, R., Blattmann, A., Lorenz, D., Esser, P., and Ommer, B. High-resolution image synthesis with latent diffusion models, 2022. URL <https://arxiv.org/abs/2112.10752>.

Stanczuk, J., Batzolis, G., Deveney, T., and Schönlieb, C.-B. Your diffusion model secretly knows the dimension of the data manifold. *arXiv preprint arXiv:2212.12611*, 2022.

Surkov, V., Wendler, C., Mari, A., Terekhov, M., Deschenaux, J., West, R., Gulcehre, C., and Bau, D. One-step is enough: Sparse autoencoders for text-to-image diffusion models. *arXiv preprint arXiv:2410.22366*, 2024.

Tang, R., Liu, L., Pandey, A., Jiang, Z., Yang, G., Kumar, K., Stenetorp, P., Lin, J., and Türe, F. What the daam: Interpreting stable diffusion using cross attention. In *Proceedings of the 61st Annual Meeting of the Association for Computational Linguistics (Volume 1: Long Papers)*, pp. 5644–5659, 2023.

Tempczyk, P., Michaluk, R., Garncarek, L., Spurek, P., Tabor, J., and Golinski, A. Lidl: Local intrinsic dimension estimation using approximate likelihood. In *International Conference on Machine Learning*, pp. 21205–21231. PMLR, 2022.

Ye, W., Zhu, H., Wang, W., Liu, Y., and Wang, M. All-in-one slider for attribute manipulation in diffusion models. *arXiv preprint arXiv:2508.19195*, 2025.

Yin, T., Gharbi, M., Park, T., Zhang, R., Shechtman, E., Durand, F., and Freeman, W. T. Improved distribution matching distillation for fast image synthesis. *arXiv:2405.14867*, 2024.

Zhang, L., Rao, A., and Agrawala, M. Adding conditional control to text-to-image diffusion models. In *Proceedings of the IEEE/CVF international conference on computer vision*, pp. 3836–3847, 2023.

A. Linearity in Semantic Latent Spaces

In this section, we provide the complete quantitative evaluation of the geometric structure of semantic transitions discussed in Section 3. To assess the validity of the linear assumption often made in latent space manipulation, we generated $N = 700$ trajectories between distinct semantic concepts.

We projected these trajectories into the CLIP visual embedding space and computed four metrics to quantify their deviation from linearity:

1. **Straightness Index:** The ratio of the Euclidean distance between the start and end points to the cumulative length of the trajectory. A value of 1.0 indicates a perfectly straight line.
2. **Average Cosine Similarity:** The mean cosine similarity between consecutive step vectors along the path.
3. **Variance Ratio (PC1):** The proportion of variance explained by the first principal component of the trajectory points.
4. **RMSE (Linear Fit):** The root mean square error of the trajectory points relative to a linear interpolation between the start and end states.

The results, presented in Table 4, demonstrate that simple linear interpolation in the text conditioning space yields highly non-linear paths in the visual embedding space, necessitating the gradient-based approach proposed in our method.

Table 4. Quantitative Analysis of Trajectory Linearity. Metrics are averaged over $N = 700$ trajectories. The “Ideal” column indicates values for a perfectly linear path. The observed negative cosine similarity and low straightness index confirm the highly non-linear nature of the latent evolution.

Metric	Observed Value	Ideal (Linear)
Avg. Cosine Similarity	-0.4696 ± 0.0590	1.0
Straightness Index	0.1696 ± 0.0180	1.0
Variance Ratio (PC1)	0.3353 ± 0.0472	1.0
RMSE (Linear Fit)	0.4271 ± 0.0254	0.0

B. Influence of the dataset size on the resulting space

In this section, we analyze the stability of the discovered semantic subspace relative to the number of gradients, N , used for decomposition. Our objective is to determine a sufficient dataset size that captures the concept's manifold without excessive computational cost.

To evaluate this, we compute the Principal Component Analysis (PCA) multiple times using varying subset sizes and compare the resulting subspaces against a reference space constructed from 50,000 gradients.

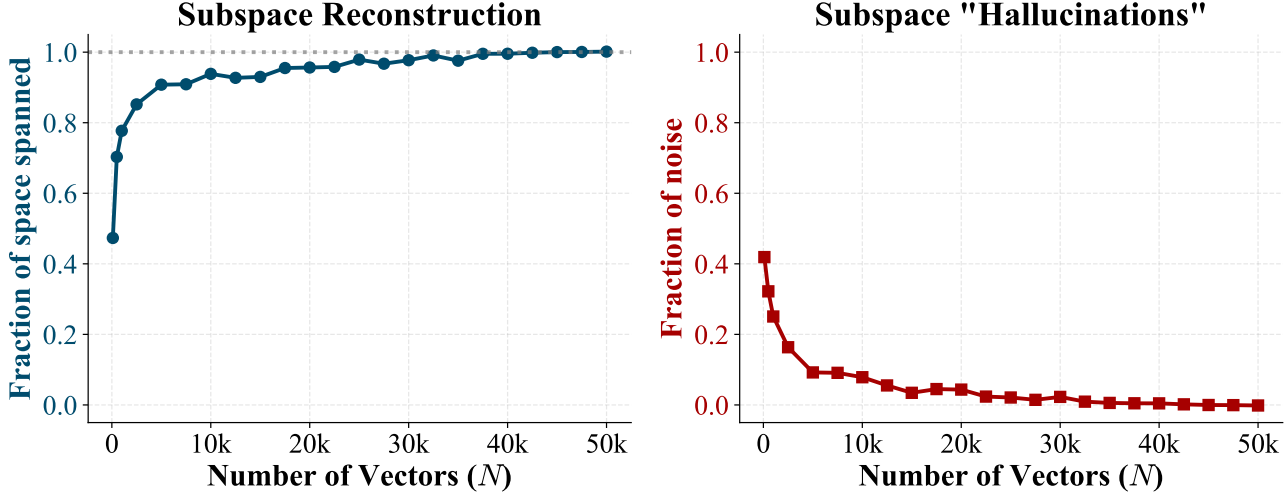


Figure 9. Influence of number of gradients on resulting subspace

As illustrated in Figure 9, the discovered subspace stabilizes rapidly as the number of vectors increases. In Figure 9 (left), we measure the fraction of subspace spanned by the smaller subset compared to the reference space. The curve shows a steep initial ascent, indicating that even a small number of gradients can capture the primary semantic directions. On the other hand in Figure 9 (right) we quantify the fraction of noise, defined as directions present in the smaller subset but absent in the reference, to ensure the discovered axes are semantically valid. This noise fraction decreases significantly as N approaches 30,000.

By comparing the trade-off between reconstruction accuracy and the reduction of "hallucinated" directions, we identify 30,000 gradients as the optimal sweet spot for our experiments. This volume provides a robust representation of the concept manifold while maintaining computational efficiency.

C. Diffusion timestep selection

One of the hyperparameter affecting the way how our method works is the selection of the diffusion timestep t at which semantic gradients are collected. In this section, we analyze how the noise level during backpropagation influences the richness and magnitude of the discovered semantic directions. Figure 10 illustrates the relationship between the diffusion timestep and the magnitude of the resulting gradient backpropagated to the specific token. We observe that gradient magnitude generally increases with t , peaking at the highest noise levels. As shown in Table 5, we quantitatively evaluated the semantic alignment of these gradients using DreamSim, DINO, and CLIP similarity metrics.

Our analysis indicates that gradients collected at high noise levels ($t \approx T$) produce the strongest CLIP and DINO similarity scores. This is in line with recent work by (Liu et al., 2024) which suggests that during the initial stages of the diffusion process, the model is most reliant on text conditioning to establish the global structure of the image. While the DreamSim distance remains relatively consistent across various timesteps, there is a marginal improvement as t increases, which points toward more precise semantic transitions. Based on these observations, we identified the late denoising stages as the optimal spot for capturing the most semantically rich and steerable directions within the embedding space

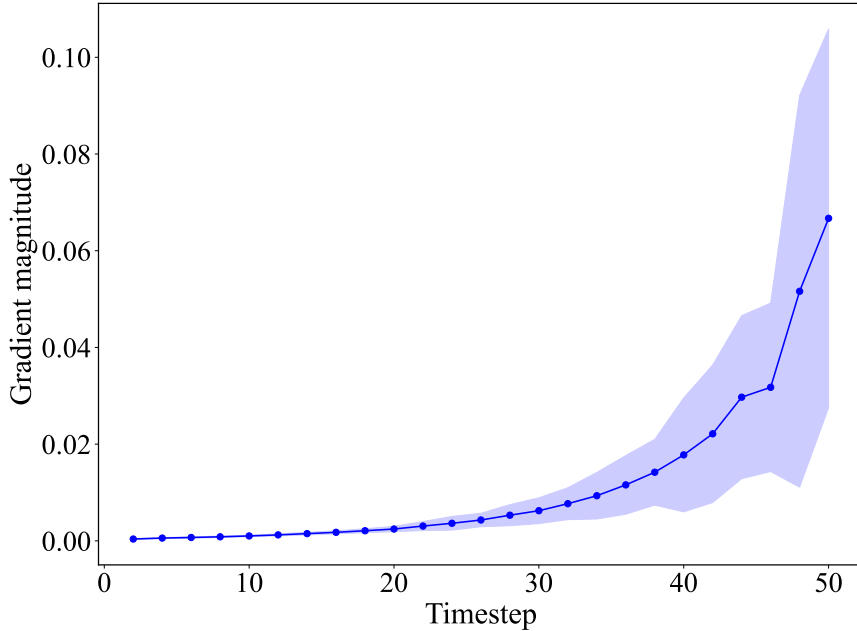


Figure 10. Gradient Magnitude across Diffusion Timesteps. The evolution of semantic signal strength relative to the denoising schedule. The increase in gradient magnitude at higher timesteps suggests that the model’s receptivity to text-based conditioning is most significant during the early stages of generation, where the high noise floor requires the conditioning signal to define the core semantic layout.

Timestep	DreamSim (\downarrow)	DINO (\uparrow)	CLIP (\uparrow)
36	0.415	0.485	0.781
40	0.415	0.488	0.782
43	0.415	0.486	0.783
46	0.407	0.491	0.785
50	0.404	0.502	0.791

Table 5. Average (across 500 pairs) DreamSim distance, DINO similarity, and CLIP similarity between image changed by a gradient from the corresponding timestep and the image towards which the gradient is pointing. Arrows indicate the direction of better performance.

D. Generalization to Transformer-based Models

To evaluate the architectural agnosticism of ELROND, we extended our experiments to Flux Schnell, a state-of-the-art transformer-based diffusion model. As illustrated in Figure 11, our method successfully identifies semantically rich and steerable directions within the conditioning space of the transformer architecture. The discovered directions for the tested concepts show high levels of semantic coherence including different styles of cars, textures/breeds of dogs or demographic and environmental attributes. Interestingly, our method was also able to discover composition-related features like the pose of a dog (lying), or a person (from behind).

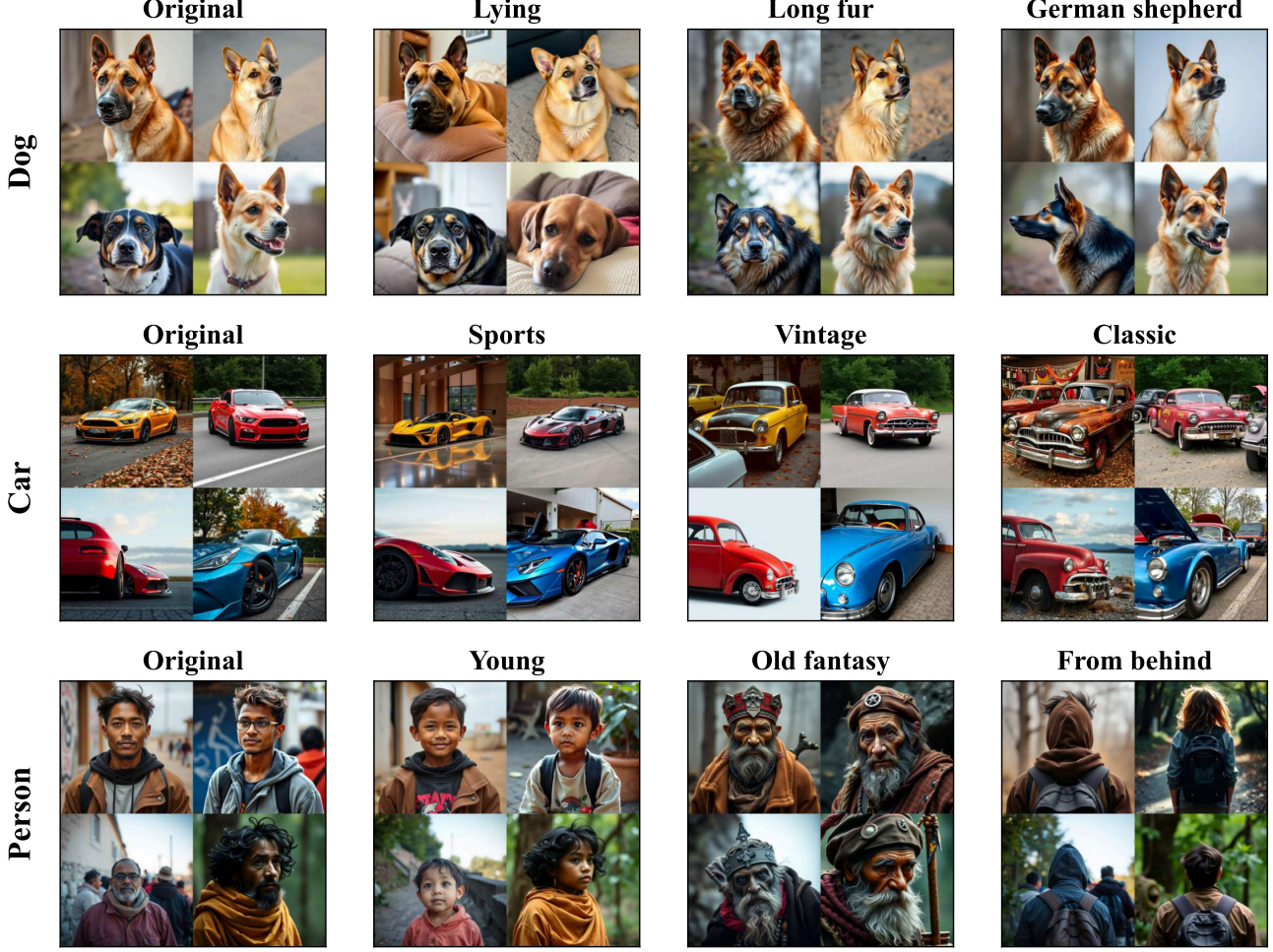


Figure 11. Generalization to Transformer-based Architectures. ELROND effectively extracts semantically coherent latent directions from Flux Schnell, a transformer-based diffusion model. The discovered directions for Dog, Car, and Person show high levels of interpretability.

E. Analysis of Failure Cases and Limitations

As discussed in the limitations section, the decomposition of the gradient dataset \mathcal{G} can occasionally yield directions that lack clear human interpretability. As visualized in Figure 12, these failure modes typically fall into two categories:

- Perceptually Inert Directions: Modulations that, despite a non-zero norm, fail to produce a significant semantic shift in the generated output.
- Unstructured Artifacts: Interventions that trigger "hallucinated" textures or chaotic pixel-level variations rather than coherent attribute transformations.

Moreover, while our method facilitates token-level steering, the contextual dependency of text embeddings can result in partial semantic leaking. Figure 13 illustrates instances where independent subject steering is compromised leading to unintended variations in non-target subjects when the magnitude of the steering vector is high.

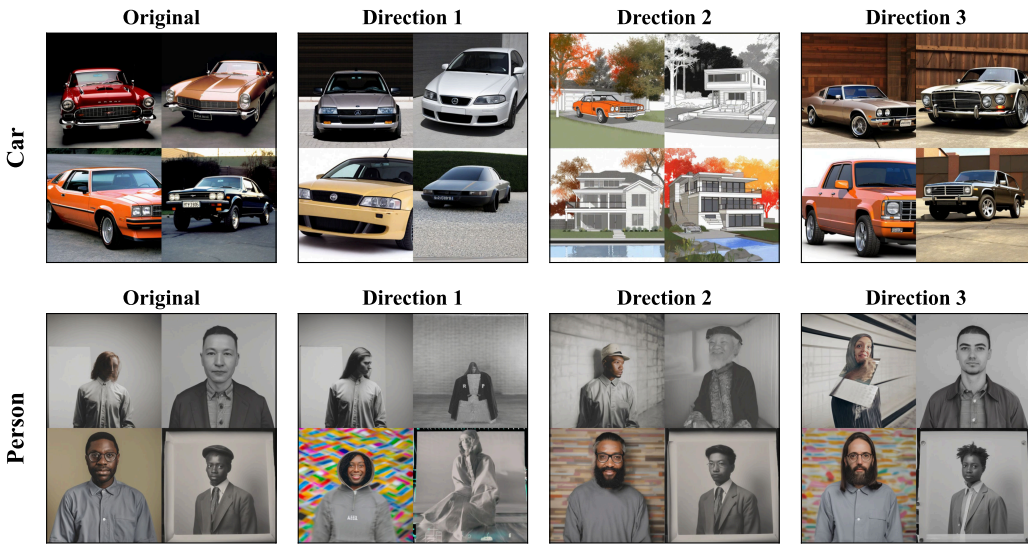


Figure 12. Failure cases for sdxl-dmd.

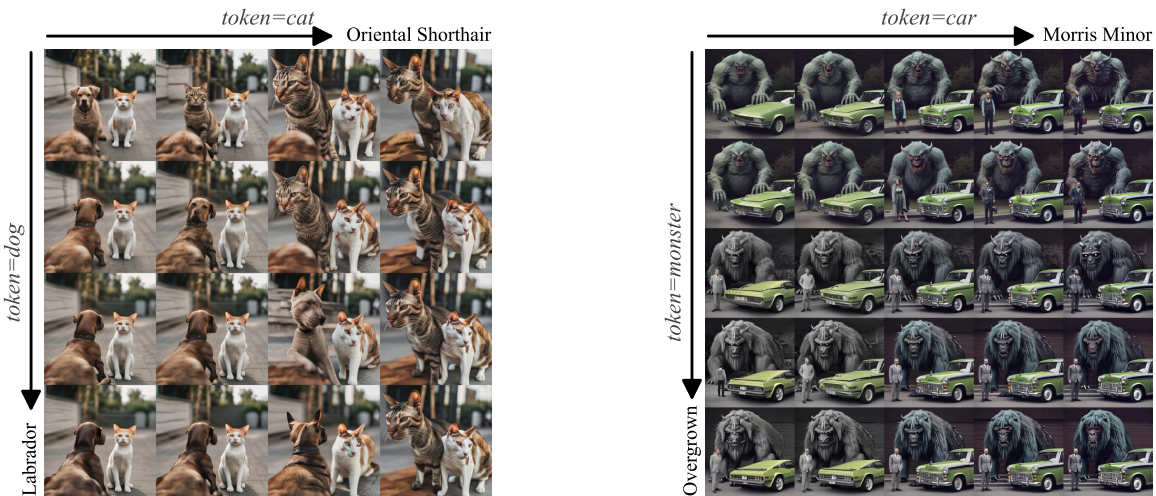


Figure 13. Applying latent directions discovered by ELROND does not always allow for a token-level composability, enabling independent steering of distinct concepts.

F. Discovered subspaces and SAE features analysis

In this section, we provide a quantitative analysis of the semantic subspaces discovered by ELROND. We compare the complexity and richness of the representations learned by the teacher model (SDXL) versus the distilled student model (SDXL-DMD) across two decomposition methods: Principal Component Analysis (PCA) and Sparse Autoencoders (SAE).

Table 6. Number of principal components found

Concept	SDXL	SDXL-DMD
Cat	83	77
Car	88	95
Monster	54	74
Dog	77	65
Person	69	66

Table 7. Number of non-dead features in the trained SAEs. All SAE have exactly 2048 features total.

Concept	SDXL	SDXL-DMD
Cat	1926	1635
Car	1954	1880
Monster	1624	1425
Dog	1864	1601
Person	1773	1854

G. Loss Functions for Semantic Gradient Calculation

A critical component of our method is the calculation of the semantic gradient $g_{i,j}$ between a source image $x^{(i)}$ and a target image $x^{(j)}$. This gradient represents the direction in the embedding space that shifts the generation from the source state toward the target state. The choice of the loss function \mathcal{L}_{sem} used to compute this gradient significantly influences the quality and steerability of the resulting semantic directions. In this section, we evaluate four different loss objective formulations to determine the optimal approach.

To assess the efficacy of different loss functions, we constructed a dataset of 200 image pairs sharing the same semantic concept (e.g., pairs of different "cats" or "cars"). For each pair (x_{src}, x_{tgt}) , we computed the gradient $\nabla_{e_{tok}} \mathcal{L}(x_{src}, x_{tgt})$ using a specific loss function. We then initiated the reverse diffusion process using the fixed noise of the source image x_{src} , but intervened in the text embedding space by injecting the calculated gradient.

The resulting generated image x_{gen} represents the model's attempt to transform x_{src} into x_{tgt} using the semantic information encoded in the gradient. We evaluated the alignment between x_{gen} and the target image x_{tgt} using three metrics: DreamSim distance (Fu et al., 2023) (perceptual similarity), CLIP similarity (semantic alignment), and DINO similarity (structural/object alignment). We compared the following four loss formulations:

1. **Mean Squared Error (MSE):** The standard reconstruction loss calculated directly between the predicted denoised latent \hat{z}_0 of the source and the latent representation of the target.
$$\mathcal{L}_{MSE} = \|\hat{z}_0^{(src)} - z_0^{(tgt)}\|_2^2 \quad (8)$$
2. **Aligned MSE:** A variant of MSE designed to mitigate spatial misalignment between the source and target objects. We utilized DAAM (Tang et al., 2023) to generate attention masks M_{src} and M_{tgt} corresponding to the concept token. We then spatially aligned the features of the target to the source based on the centroids of these masks before computing the MSE. This loss aims to penalize semantic differences while being invariant to object position.
3. **Chamfer Distance:** Treating the feature maps of the source and target latents as sets of feature vectors, we computed the Chamfer distance. This permutation-invariant metric measures the similarity between the two sets of features without enforcing strict spatial correspondence.
4. **Maximum Mean Discrepancy (MMD):** Similar to Chamfer distance, we treated the feature maps as distributions and minimized the MMD kernel distance between the source and target distributions.

The quantitative results are summarized in Table 8. We observe that the standard **MSE** loss consistently outperforms other formulations across all three metrics. It achieves the lowest DreamSim distance (0.4114) and the highest CLIP (0.8037) and DINO (0.5073) similarities.

While *Aligned MSE* performs comparably, the overhead of computing attention maps via DAAM does not yield a performance benefit over standard MSE. The distribution-based losses (*Chamfer* and *MMD*) performed significantly worse, suggesting that preserving the specific spatial structure of the latent code is crucial for extracting accurate semantic directions in the diffusion embedding space. Based on these findings, we employ standard MSE for all gradient calculations in our main method.

Table 8. Comparison of alignment metrics across different loss functions. The generated images steered by gradients derived from MSE loss exhibit the highest similarity to the target images across perceptual (DreamSim), semantic (CLIP), and structural (DINO) metrics.

Loss	DreamSim Dist. ↓	CLIP Sim. ↑	DINO Sim. ↑
MSE (Ours)	0.4114	0.8037	0.5073
Aligned MSE	0.4123	0.8021	0.5047
Chamfer Distance	0.4439	0.7837	0.4359
MMD	0.4533	0.7707	0.3928

H. Additional metrics and visual comparison

In this section, we expand our quantitative evaluation by analyzing the trade-off between the quality and diversity of the generated images using Precision and Recall metrics (Kynkäanniemi et al., 2019). Here, Precision measures the fidelity of the generated samples (i.e., how much they reside within the reference manifold of real data), while Recall quantifies the diversity coverage (i.e., how much of the reference manifold is captured by the generator).

Table 9. **Precision.** We measure the fidelity of generated samples to the reference manifold. Higher is better.

Concept	ELROND SAE (SDXL)	ELROND SAE (SDXL-DMD)	ELROND PCA (SDXL-DMD)	SDXL-DMD	SlidersSpace
Car	0.1492	0.1478	0.1331	0.1622	0.1673
Cat	0.1410	0.1331	0.0979	0.2306	0.1349
Dog	0.1154	0.1105	0.0847	0.1431	0.1901
Monster	0.0710	0.0682	0.0585	0.0559	0.0649
Person	0.0874	0.0808	0.0808	0.1169	0.1019

Table 10. **Recall.** We measure the diversity coverage of the reference manifold. Higher is better.

Concept	ELROND SAE (SDXL)	ELROND SAE (SDXL-DMD)	ELROND PCA (SDXL-DMD)	SDXL-DMD	SlidersSpace
Car	0.5179	0.4782	0.4852	0.1961	0.4672
Cat	0.5240	0.4856	0.6469	0.1243	0.4318
Dog	0.6616	0.6123	0.7218	0.2059	0.5761
Monster	0.4313	0.4793	0.5432	0.1139	0.4463
Person	0.5318	0.5598	0.5013	0.1296	0.3936

Quantifying Mode Collapse and Restoration The severity of mode collapse in the distilled SDXL-DMD model is explicitly captured by its low Recall scores in Table 10. For instance, the base SDXL-DMD achieves a Recall of only 0.2059 for the "Dog" concept, indicating that it generates a very narrow subset of the possible visual variations found in the teacher model. ELROND successfully mitigates this collapse, drastically increasing Recall across all concepts (e.g., improving "Dog" Recall to 0.7218 with SAE), thereby verifying that our method effectively restores the intrinsic diversity of the generative process.

Comparison of Decomposition Methods: SAE vs. PCA When comparing the two decomposition strategies, a distinct trade-off between geometric coverage and semantic validity emerges. The Principal Component Analysis (PCA) variant consistently yields the highest Recall scores, such as 0.7218 for "Dog" compared to 0.6123 for the Sparse Autoencoder (SAE). This outcome is expected, as PCA maximizes variance and spans the largest possible linear subspace, thereby ensuring broadly diverse outputs. Conversely, the SAE variant consistently achieves higher Precision than PCA – for example, 0.1105 versus 0.0847 for "Dog". This suggests that while PCA covers a larger volume of the latent space, it may inadvertently include "noisier" or less semantically coherent directions. In contrast, the SAE adapts to the non-uniform density of the semantic gradients. By minimizing expected reconstruction error, the SAE naturally allocates a higher density of feature vectors to regions of the manifold where the probability density of gradients is high. Consequently, sampling from the SAE dictionary effectively approximates the true underlying density of the concept, resulting in generated samples that are more faithful to the reference manifold and achieve consistently higher Precision scores (e.g., 0.1105 versus 0.0847 for "Dog").

Comparison with SliderSpace While SliderSpace achieves high Precision scores (e.g., 0.1901 for "Dog"), likely due to its reliance on stable, external CLIP-guided directions, it lags behind our approach in Recall (e.g., 0.5761 vs. 0.7218). This confirms our hypothesis that deriving directions from the model's own gradients is better suited for uncovering the full, latent diversity of the model than when constrained by external proxies.

For direct visual comparison in the following plots, we present random samples from the original models (SDXL and SDXL-DMD) and version augmented with directions from different decomposition techniques.

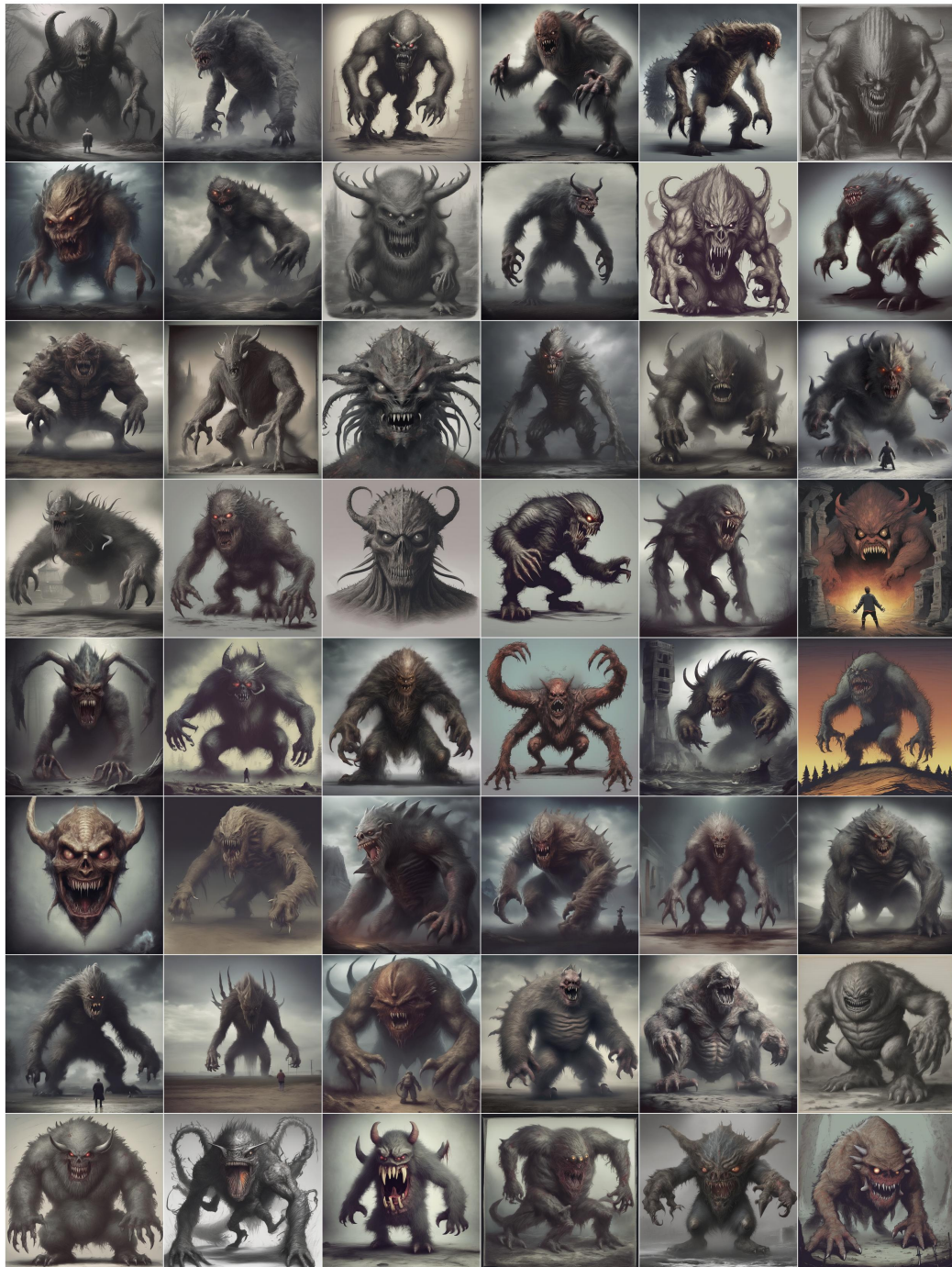


Figure 14. Uncurated samples generated by the teacher model (SDXL) for the concept "monster"

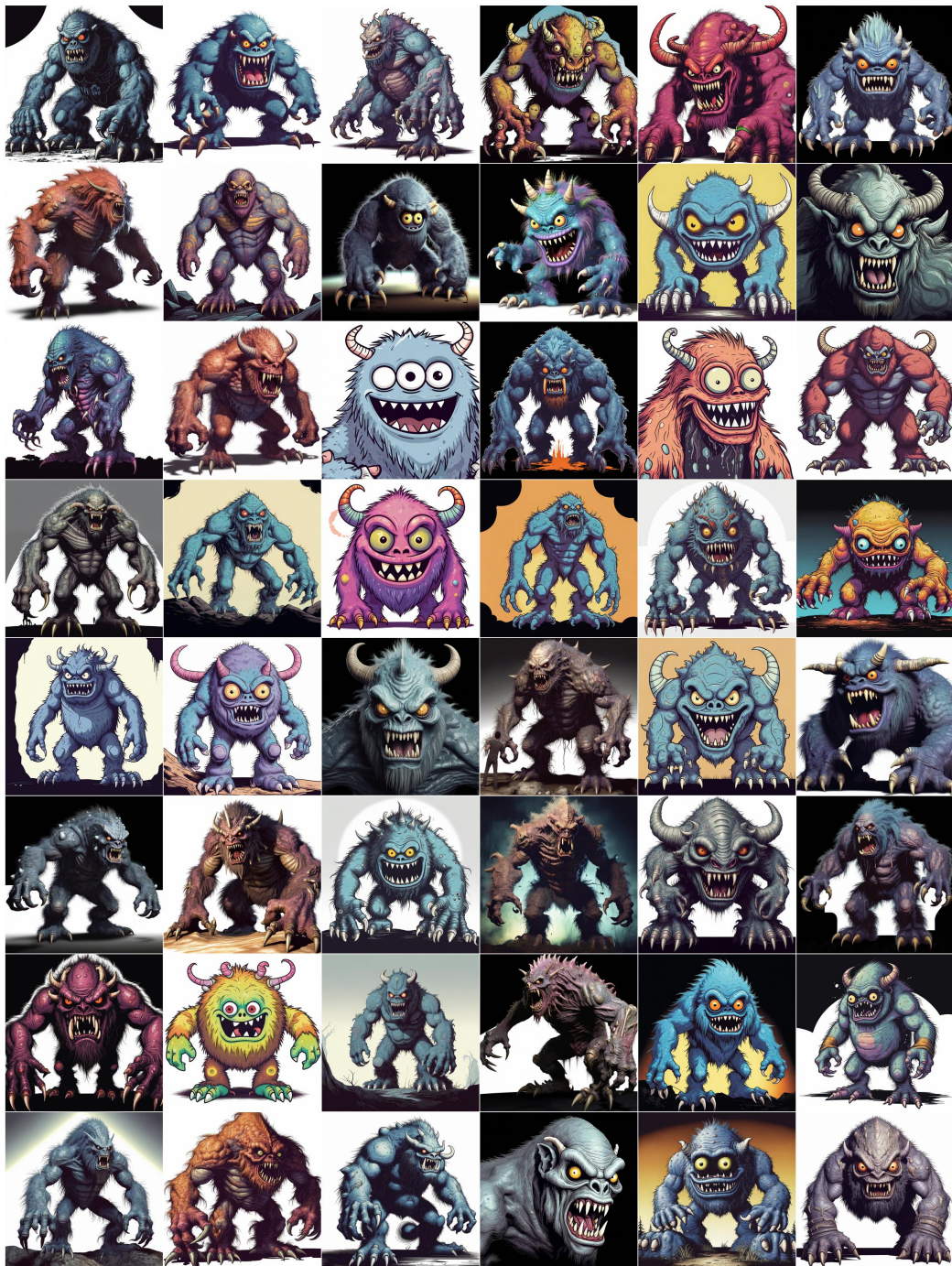


Figure 15. Uncurated samples generated by the distilled model (SDXL-DMD) for the concept "monster", illustrating the baseline performance.

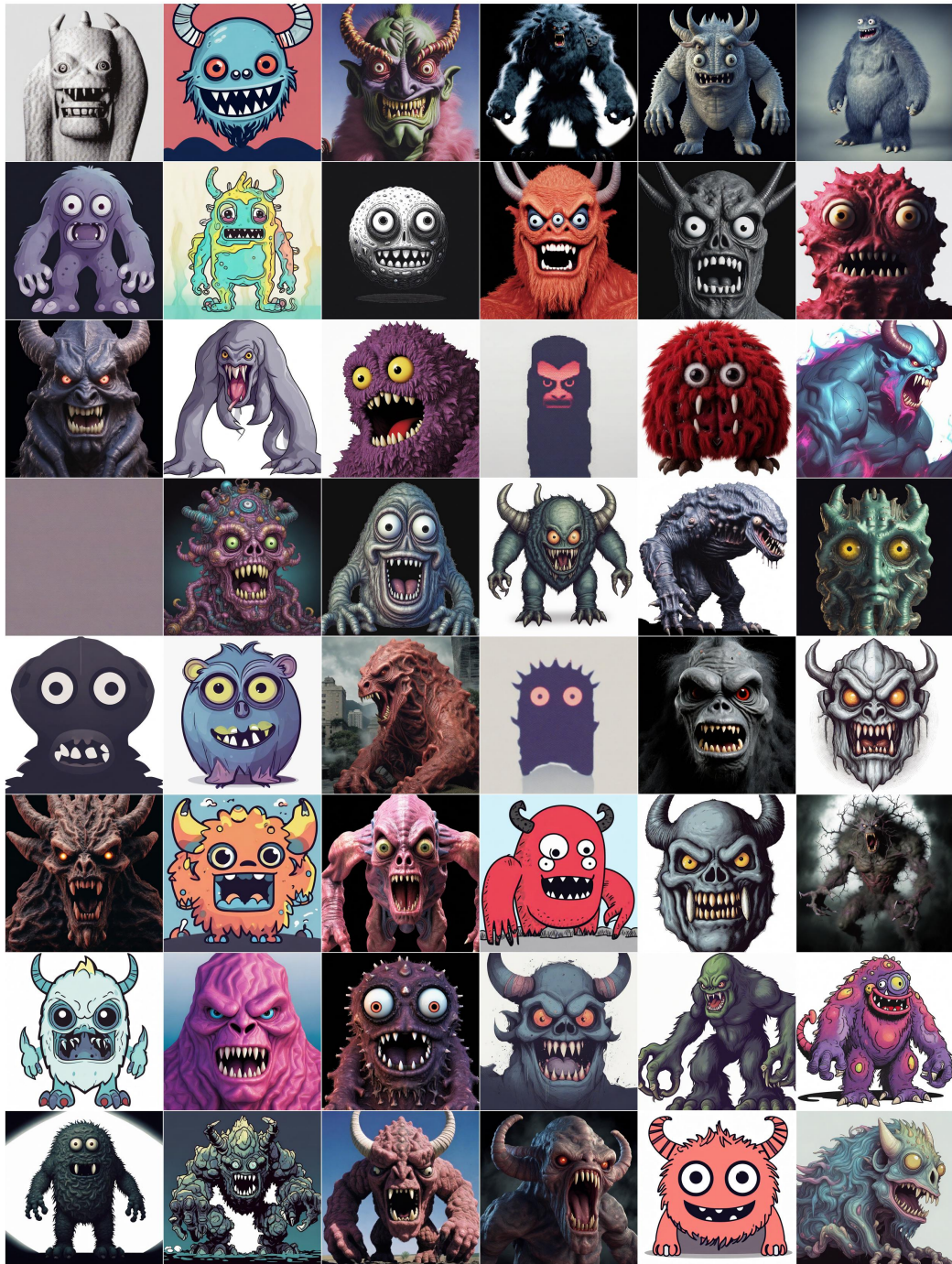


Figure 16. Samples generated by SDXL-DMD when modulated using the **SliderSpace** method.



Figure 17. Samples generated by SDXL-DMD modulated with latent directions discovered by **ELROND (PCA)** within the distilled model itself.



Figure 18. Samples generated by SDXL-DMD modulated with latent directions discovered by **ELROND (SAE)** within the distilled model itself.

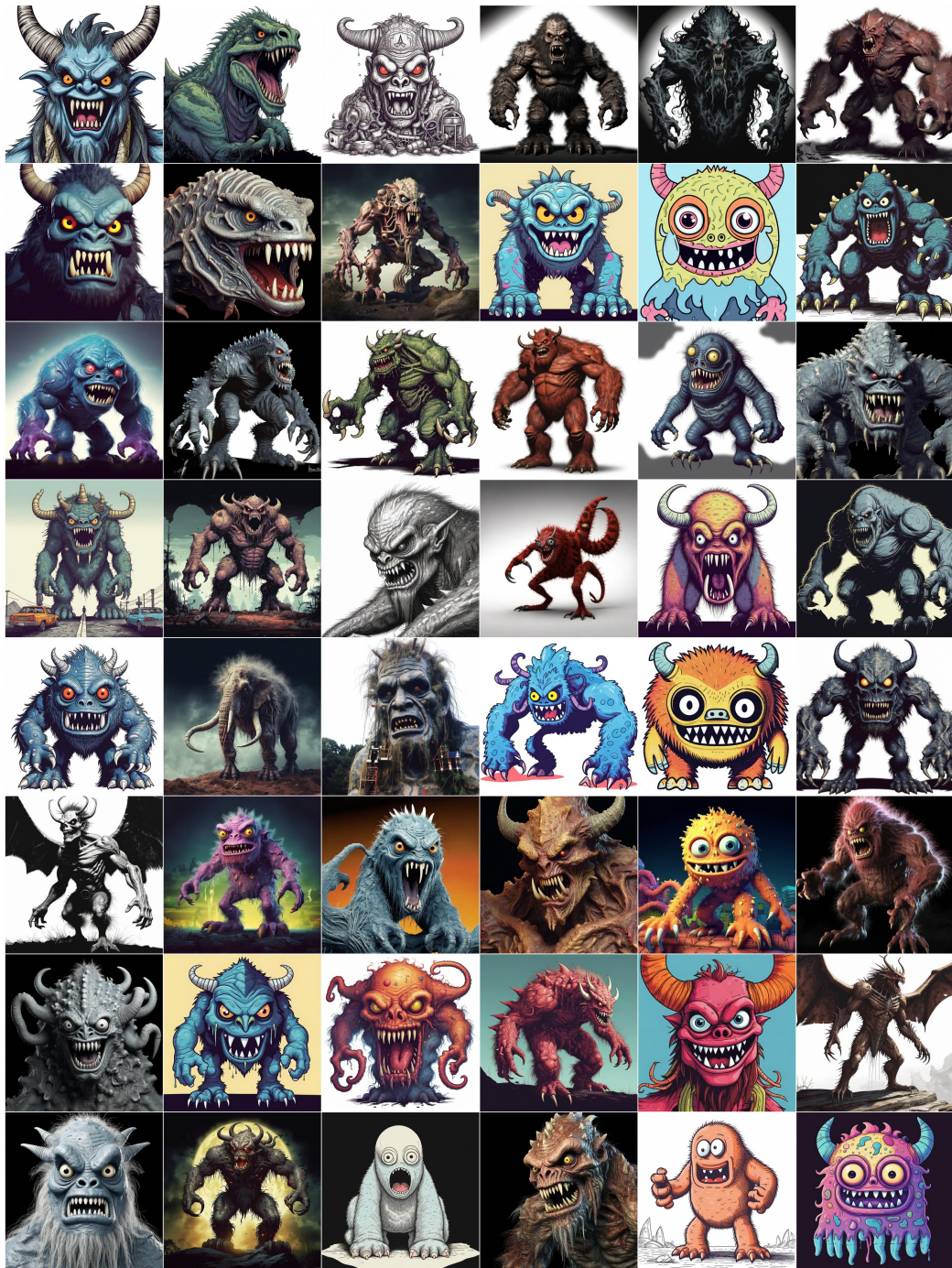


Figure 19. Samples generated by SDXL-DMD modulated with latent directions discovered by **ELROND (SAE)** within the *teacher* model (SDXL).